PHYSICAL REVIEW B **92**, 241303(R) (2015)

Hydrogenation-induced atomic stripes on the $2H$-MoS_2 surface

Sang Wook Han,[1,*,†] Won Seok Yun,[2,*] J. D. Lee,[2,‡] Y. H. Hwang,[3] J. Baik,[4] H. J. Shin,[4] Wang G. Lee,[5] Young S. Park,[5,§] and Kwang S. Kim[5]

[1]*Center for Artificial Low Dimensional Electronic Systems, Institute for Basic Science (IBS), Pohang 790-784, Republic of Korea*

[2]*Department of Emerging Materials Science, DGIST, Daegu 711-873, Republic of Korea*

[3]*School of Materials Science and Engineering, UNIST, Ulsan 689-798, Republic of Korea*

[4]*Pohang Accelerator Laboratory (PAL), Pohang 790-784, Republic of Korea*

[5]*Department of Chemistry and Physics, School of Natural Science, UNIST, Ulsan 689-798, Republic of Korea*

(Received 23 July 2015; revised manuscript received 26 November 2015; published 22 December 2015)

We report that the hydrogenation of a single crystal $2H$-MoS_2 induces a novel-intermediate phase between 2H and 1T phases on its surface, i.e., the large-area, uniform, robust, and surface array of atomic stripes through the intralayer atomic-plane gliding. The total energy calculations confirm that the hydrogenation-induced atomic stripes are energetically most stable on the MoS_2 surface between the semiconducting 2H and metallic 1T phase. Furthermore, the electronic states associated with the hydrogen ions, which is bonded to sulfur anions on both sides of the MoS_2 surface layer, appear in the vicinity of the Fermi level (E_F) and reduces the band gap. This is promising in developing the monolayer-based field-effect transistor or vanishing the Schottky barrier for practical applications.

DOI: 10.1103/PhysRevB.92.241303 PACS number(s): 73.20.−r, 64.70.Nd, 68.37.Lp, 71.15.Mb

Thickness-dependent indirect-to-direct band-gap transition of molybdenum disulfide (MoS_2) [1,2] and a successful realization of the field-effect transistor (FET) using a single-layer (1L-) MoS_2 [3] have renewed interests of transition-metal dichalcogenides. This has also boosted the development of two-dimensional (2D) materials for the high performance flexible electronic and optoelectronic devices [4,5]. For a preparation of 1L-MoS_2, the top-down exfoliation methods such as mechanical exfoliation [1–3,6], liquid exfoliation by sonication in a good solvent [7], and chemical exfoliation through lithium (Li) intercalation [8,9] are conventionally used. Among several exfoliation methods, the Li intercalation makes MoS_2 nanosheets only in the nanometer-sized metallic 1T phase [10,11], while other methods usually in the semiconducting 2H phase [1–3]. Moreover, without intercalating Li, the 1T phase can be intentionally introduced in the 2H matrix by using a high dose of incident electron beam during heating 1L-MoS_2, which accompanies intermediate phases as precursors [12]. This 2H/1T phase transition can be realized by gliding sulfur (S) and/or molybdenum (Mo) atomic planes with a change of the d-electron counts [13]. A miniaturization of 2D devices [14] plus a local induction of the metallic 1T phase [11–13] on the semiconducting 2H phase nanosheet have improved the transistor performance [15]. Further, a novel fabrication using the electron-beam-based techniques produced the semiconducting MoS_2 nanoribbons [16] and metallic nanowires [17]. In a separate method, it is notable that the hydrogenation of MoS_2 single crystal has induced a weak ferromagnetism with the improved transport property at room temperature [18]. Recently, the nanoroad prepared by the controlled (i.e., stripe-patterned) hydrogenation on the MoS_2 monolayer has been theoretically shown to be metallic [19].

In this Rapid Communication, we find a novel-intermediate phase between 2H and 1T phases, which consists of a highly-regular surface array of atomic stripes on the MoS_2 surface, and determine its materialization condition in the hydrogenation of a single crystal MoS_2. This finding motivates one to investigate the interaction between hydrogen and the MoS_2 surface based on a combination of the transmission electron microscopy (TEM), scanning photoelectron microscopy (SPEM), angle-resolved photoelectron spectroscopy (ARPES), and first-principles calculation. Further, we indicate that the electronic states associated with the emerging phase appear near the Fermi level (E_F) and reduce the band gap, promising in vanishing the Schottky barrier.

For the hydrogenation, natural single crystalline MoS_2 flakes were annealed at 300 °C for 1 h in the hydrogen gas ambient [18]. And then, for the structural characterization, the hydrogenated samples were measured by using TEM with an energy of electron beam (200 keV), which is strong enough to knock out a large number of S atoms [20,21]. However, the calculated displacement corss section for hydrogen is counterintuitively much smaller relative to that of sulfur at this energy, contrary to lower energies (<100 keV) [22], and the high resolution TEM (HRTEM) image can be taken at this condition. In order to understand how hydrogen interacts with the MoS_2 surface, SPEM and ARPES were performed at the 8A1 and 8A2 undulator beamlines of the Pohang Accelerator Laboratory (*PAL*), respectively. For the SPEM measurement, MoS_2 samples were cleaved in the UHV chamber (8×10^{-10} Torr) and annealed at 300 °C for 1 h, together with exposing to the hydrogen gas (H_2 annealing) with a pressure of 1×10^{-6} Torr, respectively. For the ARPES measurement, (i) pristine samples were also cleaved in the UHV chamber (3×10^{-9} Torr), (ii) exposed to the hydrogen gas for 1 h (1×10^{-6} Torr), and (iii) postannealed at 300 °C for 1 h. In order to investigate 1L- and 2L-MoS_2 with and without the H-S bonding, the density functional theory (DFT) calculations were performed

*These authors contributed equally to this work.

†Present address: Department of Physics and EHSRC, University of Ulsan, Ulsan 680-749, Republic of Korea.

‡Corresponding author: jdlee@dgist.ac.kr

§Corresponding author: ysinpark@unist.ac.kr

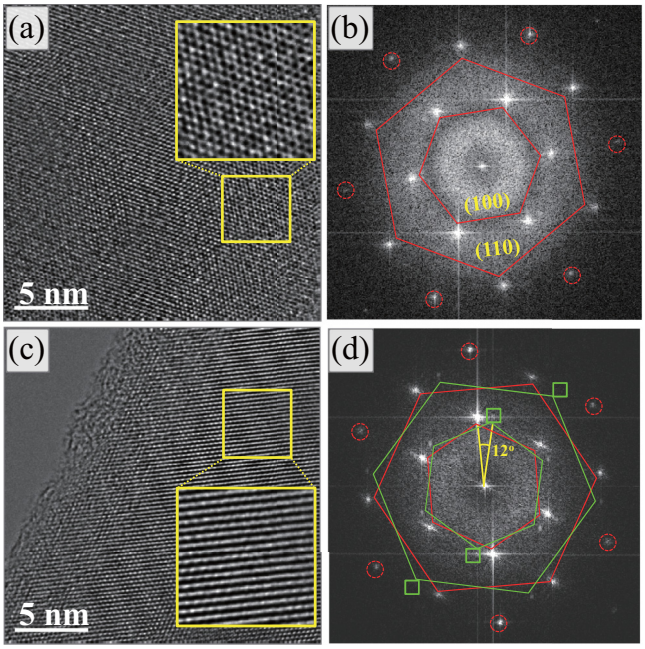

FIG. 1. (Color online) (a) HRTEM image of the pristine MoS_2. (b) FFT image displays hexagonally arranged spots with 1×1 structure. Inner and outer hexagons correspond to the (100) and (110) planes, respectively. (c) HRTEM image of the hydrogenated MoS_2. (d) Each plane in the FFT image consists of two (red and green) hexagons, which are rotated to each other by an angle of 12°. Weak or negligible spots are indicated by the squares at each plane. Each inset (enlarged from a selected rectangular region) of (a) and (c) manifests the typical honeycomb lattice of MoS_2 and the well-ordered surface array of atomic stripes. Six (red) dotted circles of (b) and (c) correspond to the (200) plane.

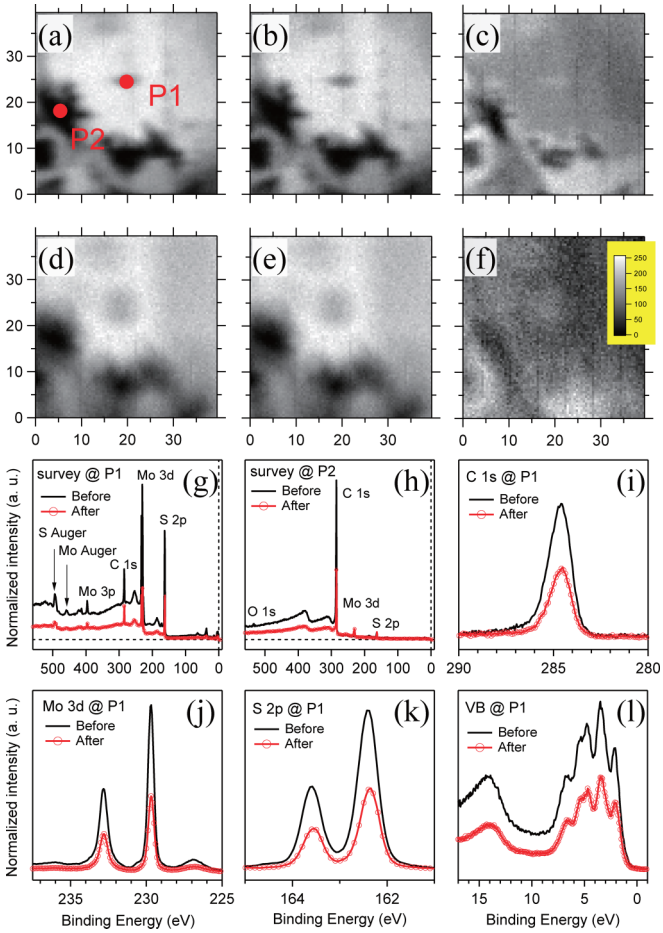

FIG. 2. (Color online) (a)–(f) Fine SPEM images of the MoS_2 surface ($40 \times 40\ \mu m^2$) before [(a)–(c)] and after [(d)–(f)] the H_2 annealing by using the selected energy channels, i.e., available for the Mo 3*d* (left panel), S 2*p* (middle panel), and C 1*s* (right panel) photoemission. (g)–(l) Wide-scan, core-level, and valence-band photoemission spectra before and after the H_2 annealing at the spots of P1 (bright) and P2 (dark) of (a).

using the projector augmented wave method as implemented in the Vienna *ab initio* simulation package (VASP) [23]. Exchange and correlation interactions between electrons were described with the generalized gradient approximation formulated by the Perdew-Burke-Ernzerhof functional [24]. All the atomic positions for the considered systems were fully optimized using the conjugate gradient method and the van der Waals (vdW)-corrected functional was employed (see Supplemental Material for details [25]).

Figure 1(a) shows the HRTEM image of a pristine MoS_2 involving numerous defects, where especially line defects can be formed from a large number of S vacancies which were knocked out by the high-energy electron beam [20,21]. A fast Fourier transform (FFT) pattern displays hexagonally arranged spots with 1×1 structure having the sixfold symmetry as shown in Fig. 1(b). The inner and outer circles indicate the MoS_2 (100) and (110) planes, which belong to the same $\{\bar{1}100\}$ and $\{\bar{2}110\}$ families [26], with the lattice spacings of 2.71 ± 0.01 Å and 1.58 ± 0.01 Å, respectively. A distinction of two planes (in their brightness) is due to various defects on the pristine MoS_2 surface.

On the other hand, the HRTEM image of the hydrogenated MoS_2 sample [Fig. 1(c)] exhibits the large-area and uniform surface array of atomic stripes. The corresponding FFT pattern in Fig. 1(d) demonstrates two (red and green) hexagon groups rotated to each other by an angle of 12°, which is attributed to the emerging well-ordered surface array over the subsurface layers remaining in the initial hexagonal pattern. The lattice spacings of (100) and (110) planes increased to 2.74 ± 0.01 Å and 1.60 ± 0.01 Å, respectively, compared to those of the pristine MoS_2. An enlarged image [inset of Fig. 1(c)] clearly shows the well-ordered surface array of atomic stripes, which are definitely different from the honeycomb lattice ($a = 3.12$ Å) [10–12] of the pristine [inset of Fig. 1(a)]. Despite the knock-on damage at the current TEM condition [20,21], this stable pattern indicates that the surface array is quite robust on the MoS_2 surface. Here in order to understand how the MoS_2 surface interacts with the hydrogen gas, we performed *in situ* SPEM measurements (Figs. S1– S3) [25].

Figures 2(a)–2(f) show the SPEM images of the MoS_2 surface ($40 \times 40\ \mu m^2$). The cleaved MoS_2 surface [Figs. 2(a)–2(c)] shows the several (dark) morphological defects due to an inefficient cleavage in the UHV chamber [25]. These dark regions were decreased after the H_2 annealing [Figs. 2(d)–2(f)]. Accordingly, as shown in Figs. 2(g)–2(l), all the intensities of micro-photoelectron spectroscopy (μ-PES) spectra including

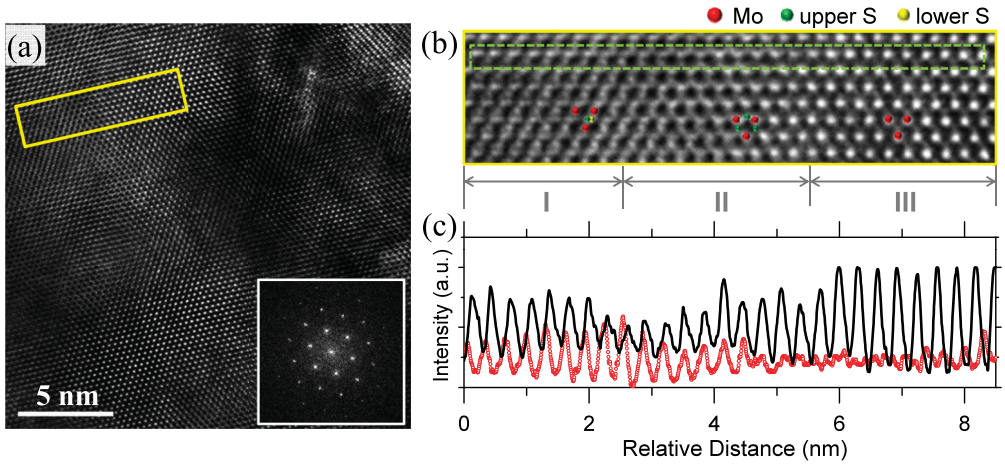

FIG. 3. (Color online) (a) HRTEM image obtained after *in situ* SPEM measurement of Fig. 2. Inset shows a FFT pattern. (b) TEM image is enlarged from a (yellow) rectangular region of (a) and roughly divided into three sectors I, II, and III, depending on the atomic configurations. (c) TEM intensity profiles along the Mo (black solid lines) and S (red dotted lines) positions, respectively, in the (green) dotted box of (b).

the C 1*s* spectrum have been reduced almost in half after the H_2 annealing. These results confirm that the hydrogen gas evidently interacts with the MoS_2 surface even though the surface is thought to be inert unlike the catalytically active edge sites [27]. It is notable that an existence of carbon after the H_2 annealing implies that a formation of the hydrocarbon (C-H bonds) [28] was inevitable during the hydrogenation at the condition of Fig. 1(c) [18].

After *in situ* SPEM measurement, TEM measurement was also performed [Fig. 3(a)]. The FFT pattern [inset of Fig. 3(a)] shows a clearer hexagonal geometry than those of the pristine and hydrogenated MoS_2 samples (Fig. 1), with less amorphous features. This means that thermal annealing of the MoS_2 surface in the UHV chamber leads to be more stable to the electron irradiation. The enlarged TEM image [Fig. 3(b)] from a (yellow) rectangular region of Fig. 3(b) comprises three sectors depending on the appropriately defined atomic configurations. In sector I of Fig. 3(b), the atomic stripes are clearly observed. This pattern is found to be transformed from the 2H phase (sector II) through gliding of the upper S plane on the MoS_2 surface, which is captured by a phase difference arising between upper (black solid) and lower (red dotted) lines as going from sector II to I in Fig. 3(c). Meanwhile, sector III may be attributed to the removal of upper S atoms from the 2H phase because of the high-energy electron beam or thermal annealing. This can be also understood from Fig. 3(c), where the TEM signal intensities from Mo (black solid lines are appreciably enhanced and those from S (red dotted lines) are suppressed when going from sector II to III.

Now let us focus on a collection of the atomic stripes, which is a novel phase emergent on the H_2 annealed 2*H*-MoS_2 surface. Figure 4(a) enlarges a part of sector I of Fig. 3(b) and displays an apparent anisotropy between the TEM images along the L1 and L2 directions; in other words, the geometry supporting the atomic stripes. Then Fig. 4(b) provides the TEM signal profiles clearly distinct between, along the L1 and L2 directions, being consistent with Fig. 4(a). Furthermore, in order to clarify an influence of the hydrogen interaction on the electronic structure of the MoS_2 surface, the surface-sensitive ARPES measurements were also performed on the cleaved MoS_2 surface (i), on the surface exposed to the hydrogen gas for 1 h at room temperature (ii), and then on the postannealed surface at 300 °C for 1 h (iii). Figure 4(c) shows the valence-band spectra obtained from an integration of the ARPES data, where the spectrum labeled (ii) shifts the valence band maximum (VBM) toward the high binding energy side compared to the spectrum (i) [29] and the spectrum (iii) eventually shifts VBM toward E_F (0.3 eV). This hydrogenation-induced reduction of band gap is also ascertained from the optical absorption measurements and

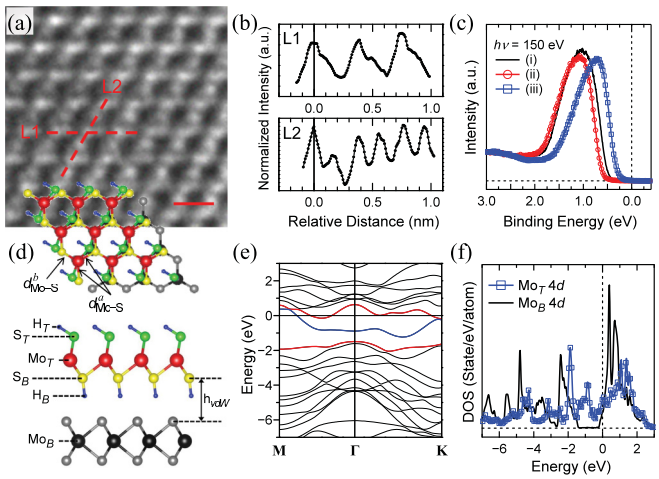

FIG. 4. (Color online) (a) Enlarged HRTEM image of the part belonging to sector I of Fig. 3(b). An anisotropy between, along the L1 and L2 directions is obvious. (b) TEM signal profiles different between, along the L1 and L2 directions. (c) Comparison of valence band spectra at the stages (i), (ii), and (iii) (see the text), which were integrated from the ARPES data. (d) Theoretical atomic configuration, obtained from the full atomic relaxation, is overlapped on the TEM image of (a). Top and side views of 2L-MoS_2 with H-S bondings on both sides of S planes of the top layer. The corresponding electronic band structure and calculated density of states (DOS) are illustrated in (e) and (f), respectively. The DOS corresponds to the integral of electronic band structure of (e).

TABLE I. Comparison of TEM (Figs. 1 and 4) and DFT results (Fig. 4) for the lattice constant (a), lattice spacing of the (100) plane [i.e., $d(100)$], and bond lengths. All lengths are shown in Å. (i) and (ii) indicate the 2L- and 1L-MoS_2 with H-S bonding on both sides of S planes of the top layer.

TEM	a	$d(100)$	DFT	a	$d^a_{Mo_T\text{-}S_T}$	$d^a_{Mo_T\text{-}S_B}$	$d^b_{Mo_T\text{-}S_T}$	$d^b_{Mo_T\text{-}S_B}$
Fig. 1(a)	3.12	2.71	1L-MoS_2	3.184	2.413			
Fig. 1(c)		2.74	2L-MoS_2	3.165	2.410	2.411		
Fig. 4(a)	3.18	2.74	Fig. 4(d)$^{(i)}$	3.230	2.487	2.364	3.118	2.312
			Fig. S6$^{(ii)}$	3.152	2.441	2.441	2.593	2.593

resolves the reason why the transport properties improve via the hydrogenation (Fig. S5) [25].

In Fig. 4(d), the atomic configuration theoretically calculated from the full atomic relaxation is nicely overlapped on the atomic stripes of the TEM image [Fig. 4(a)]. We considered possible configurations of the H-S bonding on two (upper and lower) S planes of 1L-MoS_2 (Fig. S6) [25] and of the top layer of 2L-MoS_2 [Fig. 4(d)]. Compared to the pristine slabs, the H-S bonding increases the lattice constant of 2L-MoS_2 by 2.1%, while it decreases 1L-MoS_2 by 1.0% (see Table I). In details, while $d^a_{Mo_T\text{-}S_T}$ and $d^b_{Mo_T\text{-}S_T}$ of 2L-MoS_2 increase by 3.2% and 29.4%, respectively, $d^a_{Mo_T\text{-}S_B}$ and $d^b_{Mo_T\text{-}S_B}$ decrease by 1.9% and 4.1%, respectively. Particularly, $d^b_{Mo_T\text{-}S_T} \gg d^a_{Mo_T\text{-}S_T}$ implies that the atomic stripes are likely formed in 2L-MoS_2. The H_B-S_B bond of 2L-MoS_2 [Fig. 4(d)] is oriented out of plane due to the vdW interaction [30]. That is, only the topmost S_T plane glides along the direction of the H_T-S_T bond, which is distinguishable from 1L-MoS_2 (Fig. S6) [25]. This is actually in good agreement with the experimental observation of the stripes [Figs. 1(c) and 4(a)]. In Fig. 4(e), the upper and lower bands (red) near E_F originated from the Mo $4d$ and S $3p$ states of 2L-MoS_2 constitute the conduction band minimum (CBM) and VBM, respectively, while the intermediate impurity (blue) band between the CBM and VBM is contributed from the hydrogenation. Hence, a formation of the H-S bond induces the atomic stripes, which is attributed to an impurity band at E_F [Fig. 4(e)] indicating the metallization of the top layer [19,31]. It is then understood that the stripes perform the quasi-one-dimensional conduction. In Fig. 4(f), Mo_T implies the molybdenum on the hydrogenated top layer with a closed band gap and Mo_B the bottom layer with the band gap of ~1.2 eV. This closing of band gap is quite consistent with the valence-band spectrum (iii) [Fig. 4(c)], the shift of VBM toward E_F, and the optical absorption spectra (Fig. S5) [25].

Another insight relevant to the experimental realization of atomic stripes comes from the total energy consideration of the hydrogenated 2L-MoS_2 with a continuous structural change from 2H to 1T phase, as displayed in Fig. 5. In the figure, x denotes the relative position of the S_T plane between $x = 0$ (2H) and $x = 1$ (1T). An in-between value of x possibly implies the stripe phase in Fig. 5(a). It is found that, in the total energy of Fig. 5(b), the hydrogenated 2L-MoS_2 with $x \sim 0.3$ is even lower than the 2H phase ($x = 0$) and energetically most allowable. This certainly supports the present experimental observation. A comparison between TEM images of Figs. 1(c) and 3(a) [Fig. 4(a)] indicates that the size of the hydrogenated stripe phase (i.e., intermediate phase) area increases or covers the whole surface area according to an abundant supply of hydrogen gas when the different vacuum conditions between those TEM images are taken into account.

In conclusion, we reveal that the hydrogenation of the MoS_2 single crystal induces the large-area and robust surface array of atomic stripes on the MoS_2 surface, corresponding to a novel intermediate phase between 2H and 1T phases. Through the investigation combining several state-of-the-art measurements, the novel stripe phase is found to be driven by the gliding of the topmost sulfur plane due to the hydrogenation. Electronic states associated with the atomic stripes on the MoS_2 surface

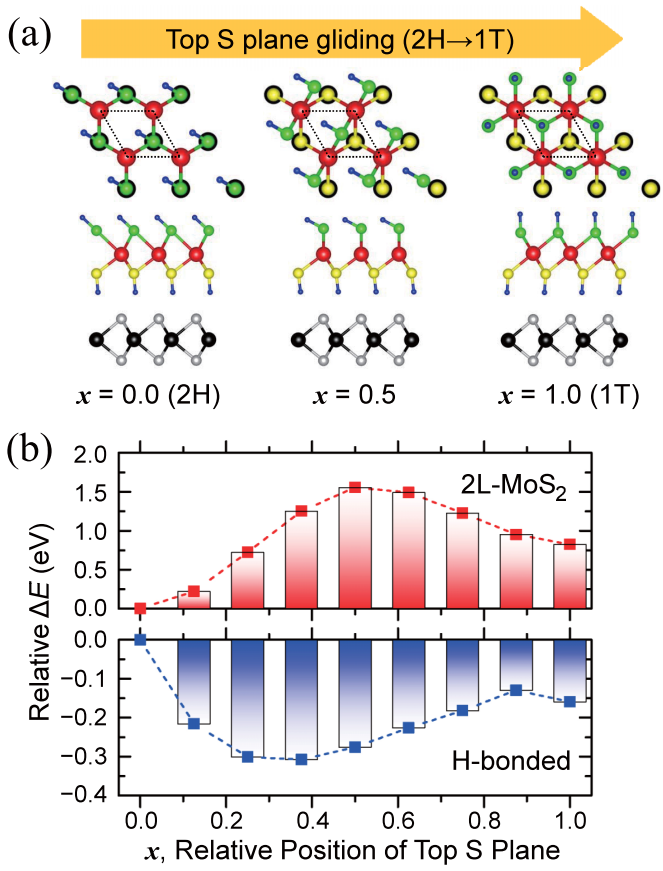

FIG. 5. (Color online) (a) Top and side views of 2L-MoS_2 for the phase transition from 2H to 1T phase, where H-S bondings are on both sides of (upper and lower) S planes of the top layer. Here, x indicates the relative position of the top S plane between $x = 0$ (2H phase) and $x = 1$ (1T phase). (b) Relative total energy differences as a function of x for 2L-MoS_2 without (upper) and with (lower) the H-S bonding as shown in (a), respectively. For each system, the total energy of 2H phase is set to zero as the reference energy.

appear in the vicinity of Fermi level (E_F), promising to attain a vanishing Schottky barrier. Understanding and controlling the interaction of hydrogen with the MoS_2 surface at the atomic scale will open nanotailoring capabilities toward advanced applications in nanoelectronics.

This work was supported by Institute for Basic Science. Works at the UNIST, DGIST, and University of Ulsan were also supported by the Ministry of Science, ICT, Future Planning, Basic Science Research Program, Priority Research Centers, and National Honor Scientist Program through the National Research Foundation of Korea (NRF) funded by the Ministry of Education (Grants No. 2013R1A1A2011426, No. 2013R1A1A2007388, No. 2010-0020414, No. 2009-0093818, and No. 2014R1A1A2003970). Experiments at PLS were supported by MSIP and PAL of Korea.

[1] A. Splendiani, L. Sun, Y. Zhang, T. Li, J. Kim, C.-Y. Chim, G. Galli, and F. Wang, Nano Lett. **10**, 1271 (2010).
[2] K. F. Mak, C. Lee, J. Hone, J. Shan, and T. F. Heinz, Phys. Rev. Lett. **105**, 136805 (2010).
[3] B. Radisavljevic, A. Radenovic, J. Brivio, V. Giacometti, and A. Kis, Nat. Nanotechnol. **6**, 147 (2011).
[4] Q. H. Wang, K. Kalantar-Zadeh, A. Kis, J. N. Coleman, and M. S. Strano, Nat. Nanotechnol. **7**, 699 (2012).
[5] M. Xu, T. Liang, M. Shi, and H. Chen, Chem. Rev. **113**, 3766 (2013).
[6] K. S. Novoselov, D. Jiang, F. Schedin, T. J. Booth, V. V. Khotkevich, S. V. Morozov, and A. K. Geim, Proc. Natl. Acad. Sci. U.S.A. **102**, 10451 (2005).
[7] J. N. Coleman *et al.*, Science **331**, 568 (2011).
[8] Z. Zeng, Z. Yin, X. Huang, H. Li, Q. He, G. Lu, F. Boey, and H. Zhang, Angew. Chem., Int. Ed. Engl. **50**, 11093 (2011).
[9] G. Eda, H. Yamaguchi, D. Voiry, T. Fujita, M. Chen, and M. Chhowalla, Nano Lett. **11**, 5111 (2011).
[10] G. Eda, T. Fujita, H. Yamaguchi, D. Voiry, M. Chen, and M. Chhowalla, ACS Nano **6**, 7311 (2012).
[11] L. Wang, Z. Xu, W. Wang, and X. Bai, J. Am. Chem. Soc. **136**, 6693 (2014).
[12] Y.-C. Lin, D. O. Dumcenco, Y.-S. Huang, and K. Suenaga, Nat. Nanotechnol. **9**, 391 (2014).
[13] M. Kertesz and R. Hoffmann, J. Am. Chem. Soc. **106**, 3453 (1984).
[14] G. Fiori, F. Bonaccorso, G. Iannaccone, T. Palacios, D. Neumaier, A. Seabaugh, S. K. Banerjee, and L. Colombo, Nat. Nanotechnol. **9**, 768 (2014).
[15] R. Kappera, D. Voiry, S. E. Yalcin, B. Branch, G. Gupta, A. D. Mohite, and M. Chhowalla, Nat. Mater. **13**, 1128 (2014).
[16] X. Liu, T. Xu, X. Wu, Z. Zhang, J. Yu, H. Qiu, J.-H. Hong, C.-H. Jin, J.-X. Li, X.-R. Wang, L.-T. Sun, and W. Guo, Nat. Commun. **4**, 1776 (2013).
[17] J. Lin *et al.*, Nat. Nanotechnol. **9**, 436 (2014).
[18] S. W. Han, Y. H. Hwang, S.-H. Kim, W. S. Yun, J. D. Lee, M. G. Park, S. Ryu, J. S. Park, D.-H. Yoo, S.-P. Yoon, S. C. Hong, K. S. Kim, and Y. S. Park, Phys. Rev. Lett. **110**, 247201 (2013).
[19] Y. Cai, Z. Bai, H. Pan, Y. P. Feng, B. I. Yakobson, and Y.-W. Zhang, Nanoscale **6**, 1691 (2014).
[20] H.-P. Komsa, J. Kotakoski, S. Kurasch, O. Lehtinen, U. Kaiser, and A. V. Krasheninnikov, Phys. Rev. Lett. **109**, 035503 (2012).
[21] H.-P. Komsa, S. Kurasch, O. Lehtinen, U. Kaiser, and A. V. Krasheninnikov, Phys. Rev. B **88**, 035301 (2013).
[22] S. T. Skowron, I. V. Lebedeva, A. M. Popov, and E. Bichoutskaia, Nanoscale **5**, 6677 (2013).
[23] G. Kresse and J. Furthmüller, Phys. Rev. B **54**, 11169 (1996); G. Kresse and D. Joubert, *ibid.* **59**, 1758 (1999).
[24] J. P. Perdew, K. Burke, and M. Ernzerhof, Phys. Rev. Lett. **77**, 3865 (1996).
[25] See Supplemental Material at http://link.aps.org/supplemental/10.1103/PhysRevB.92.241303 for the details of sample preparation, TEM, SPEM, ARPES, and DFT calculations.
[26] J. Brivio, D. T. L. Alexander, and A. Kis, Nano Lett. **11**, 5148 (2011).
[27] T. F. Jaramillo, K. P. Jørgensen, J. Bonde, J. H. Nielsen, S. Horch, and I. Chorkendorff, Science **317**, 100 (2007).
[28] I. Luciu, R. Bartali, and N. Laidani, J. Phys. D: Appl. Phys. **45**, 345302 (2012).
[29] Q. Yue, Z. Shao, S. Chang, and J. Li, Nano Res. Lett. **8**, 425 (2013); Hydrogen exposure (ii) moves the VBM away from E_F. This is contrasting with this reference that the physisorbed H_2 molecules on the MoS_2 surface act as charge accepters. Further studies are needed for the elucidation.
[30] S. W. Han, H. Kwon, S. K. Kim, S. Ryu, W. S. Yun, D. H. Kim, J. H. Hwang, J.-S. Kang, J. Baik, H. J. Shin, and S. C. Hong, Phys. Rev. B **84**, 045409 (2011).
[31] I. N. Yakovkin and N. V. Petrova, Chem. Phys. **434**, 20 (2014).